Eur. Phys. J. D **41**, 467–474 (2007)
DOI: 10.1140/epjd/e2007-00016-x

THE EUROPEAN PHYSICAL JOURNAL D

Diffraction of fast metastable atoms by micrometric reflection gratings

J. Grucker[1,a], J.-C. Karam[1], F. Correia[1], F. Perales[1], G. Vassilev[1], V. Bocvarski[2], S.M. Chérif[3], J. Baudon[1], and M. Ducloy[1]

[1] Laboratoire de Physique des Lasers (UMR-CNRS 7538), Université Paris-13, Avenue J.B. Clément, 93430 Villetaneuse, France
[2] Institute of Physics-Belgrade, Pregrevica 118, 11080 Belgrade-Zemun, Serbia
[3] CNRS, Laboratoire PMTM (UPR 9001), Université Paris-13, Avenue J.B. Clément, 93430 Villetaneuse, France

Received 8 August 2006 / Received in final form 4 January 2007
Published online 31 January 2007 –

Abstract. Diffraction of thermal velocity metastable atoms by non-magnetic and magnetic reflection gratings of micrometric period has been observed. This observation is made possible by the use of an ultra narrow beam generated by metastability exchange. Grazing incidence angles are exploited to minimise the quenching of metastable atoms on the grating surface. Potential applications are beam splitting, atom holography and probing of micro-sized solid surfaces.

PACS. 03.75.-b Matter waves – 68.49.Bc Atom scattering from surfaces (diffraction and energy transfer) – 75.70.Rf Surface magnetism

1 Introduction

Since the tremendous development of laser cooling techniques, ultra cold atoms and even Bose Einstein Condensates have been intensively used in atomic physics to exhibit coherent properties of an atom ensemble. The reason for this is that the cooling process provides atomic samples with some remarkable coherence properties (in particular, the de Broglie (dB) wavelength of cold atoms can be of several μm). One example is atomic diffraction in the reflection mode (so-called atom holography) that had been demonstrated by Shimizu and Fujita [1] using falling ultra cold metastable neon atoms ($2p^5 3s$, $^3P_0$) with a mean velocity of 3 m s^{-1}.

In this article, we demonstrate that the use of ultra cold atoms is not essential to observe atomic diffraction by micro-period reflection gratings. This is important because micro-fabricated reflection-mode gratings for thermal velocity atoms add a new tool to the field of atom optics. Since the thirties, a number of atomic diffraction experiments have been carried out with thermal ground state atom beams (alkalis and rare gases, H_2 molecules) and oriented crystal surfaces as a diffracting object (see e.g. [2–5]). In these experiments the diffraction is due to the periodic interaction at small distances (∼0.1 nm) between the incident atom and the crystal atom lattice. On another hand, few atom optics experiments have been run with fast ground-state atoms diffracted by artificial structures of a micrometric or a nanometric size. Examples are (i) the diffraction by a 200 nm period transmission grating of sodium atoms seeded in a supersonic beam of argon and its application to atomic interferometry [6]; (ii) the determination of atom-surface van der Waals (vdW) interaction from the diffraction intensities produced by a 100 nm period transmission grating [7].

In this type of experiment the use of metastable rare gas atoms provides some important advantages: (i) such atoms are easily produced (with, actually, rather low fluxes), (ii) they are detected with a high efficiency (∼30%) and can be imaged on a position sensitive detector, (iii) the vdW atom-solid interaction at mean distance (0.5–100 nm) is more intense than for ground state species, a property that has been exploited in elastic [8,9] and inelastic [10] diffraction experiments with metastable atoms (He*, Ne*, Ar*) and a 100 nm period transmission grating. Because of the smallness of the dB wavelength (∼0.01 nm), grating-periods of a few 100 nm are needed to get resolvable diffraction peaks. Such transmission gratings are not easy to produced, fragile, rather expensive and difficult to acquire.

On the contrary, reflection gratings with periods of about 1 μm are easier to make and, as we show here, are suitable to diffract fast atoms under certain conditions. We have performed an experiment in which a metastable-atom supersonic beam (He*, Ne*, Ar*) at thermal energy ($E_0 \sim 64$ meV) is diffracted by different types of reflection gratings (magnetized or not). The evidence of

[a] e-mail: grucker@galilee.univ-paris13.fr

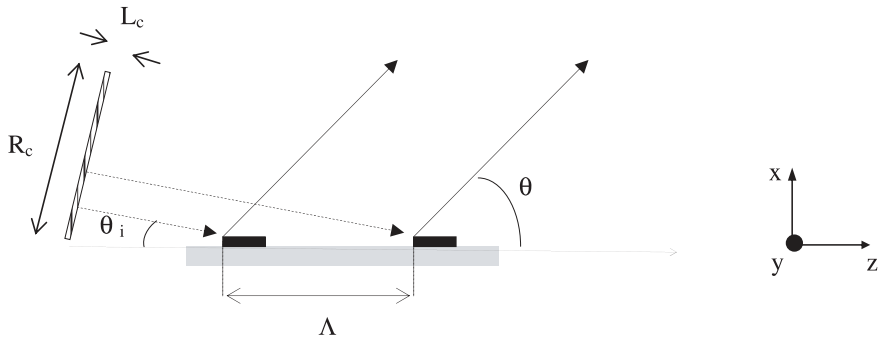

Fig. 1. Principle scheme of the experiment. The incoming He^* wave packet (transverse coherence radius R_c, longitudinal coherence length L_c) hits the grating (period Λ) at an incident angle θ_i. It is scattered in directions θ, with respect to the grating plane.

1D diffraction of fast metastable atoms is shown. Such a diffraction effect splits the initial atomic wave packet into a coherent superposition of elastically scattered wave packets. It is likely however that the coherence of this superposition is not perfect because surface roughness and random surface micro-motions are expected to induce a de-coherence especially at grazing incidence. A simulation of this effect (which will be detailed below) shows that diffraction peaks are preserved up to order 3, at least for a rms roughness magnitude not exceeding 3 nm (the manufacturer gives, for the gratings used in this work, 1–2 nm). Hence at low diffraction orders, the grating acts as a coherent beam splitter, which can then be used for atomic interferometry with reflection gratings as proposed, for example, in [11]. Similar features have already been studied in reflection-mode diffraction of atoms by evanescent light waves [12]. In Section 2, we will focus on the atomic source, then we will describe how we use its specific properties to study diffraction of metastable atoms by reflection gratings. We give here experimental details for the case of He^* atoms (1750 m/s) and report results for Ne^* (780 m/s) and Ar^* (560 m/s) atoms. Results obtained with non-magnetic and magnetic gratings are presented and discussed in Section 3. Conclusions and perspectives are given in Section 4.

2 Experiment

2.1 Atom source

Campargue-type nozzle beams [13] are characterized by a low translational temperature (a few K), leading to narrow velocity distributions, both in direction and modulus. In addition, atomic trajectories in the so-called free zone are issued from an effective source, the diameter of which is significantly smaller than that of the real nozzle (in the present case 15 μm instead of 50 μm). These remarkable properties of ground state atomic beams can be transferred, without almost any loss, to metastable atoms using the resonant metastability exchange process $He^* + He \rightarrow He + He^*$. This technique has been described in detail elsewhere [8].

For this experiment, we use such a beam of metastable Helium atoms He^*. After two collimation holes (80 μm and 100 μm, respectively located at 116 mm and 395 mm from the nozzle), we end with a beam of metastable He^* atoms ($^1S_0$, $^3S_1$) whose characteristics are as follows: the mean longitudinal velocity $\langle v \rangle$ is 1750 m s^{-1} ($\delta v/v \sim 1.5\%$ (FWHM) leading to a longitudinal δv of about 17–34 m s^{-1}) which corresponds to a longitudinal de Broglie wavelength $\lambda_\parallel = 0.057$ nm and a kinetic energy $E_0 = 64$ meV. One can then estimate the size of the atomic wave packet (the longitudinal coherence length L_c) to be $L_c = \lambda_\parallel v/\delta v$ which gives $L_c \sim 2.8$–5.7 nm for the He^* beam. The angular aperture of the beam (FWHM) is $\delta\theta \approx 0.35$ mrad which corresponds to a rms transverse velocity of 60 cm s^{-1}. Such a transverse velocity leads to a mean transverse de Broglie wavelength $\lambda_\perp \approx 163$ nm. From the value of $\delta\theta$ one can derive, using a *umbra–penumbra* method, the effective source diameter to be about 15 ± 5 μm. This relatively small diameter originates from the nozzle expansion mechanism: rectilinear atomic trajectories within the so-called "zone of silence" or "Mach bottle" seem to be issued from an effective source located at a few mm upwards the nozzle [13]. Its diameter is about 1/3 of the nozzle diameter at least when the nozzle beam is properly operating. Because of the small size of this source, an almost perfectly defined velocity vector is present at each point of the grating illuminated by the beam.

2.2 Experimental requirements

The experiment we describe here is quite simple in its principle. He^* metastable atoms are sent on a reflection grating of a few μm period and one looks at the diffraction pattern (see Fig. 1). However, the experimental realisation of such an easy principle is not trivial. In the following, we point out the main problems of such an experiment and show how we managed to overcome them.

The first limitation of this experiment is the reflection factor of metastable atoms hitting a metallic object. It is well known that metastable atoms are quenched into the ground state as soon as their outer electronic orbital overlaps the electronic orbitals of the solid [14]. The probability of this quenching process is very close to 1 as soon as the distance between the surface (here the grating) and the metastable atom (here He^*) is less than 1 nm. Nevertheless, even at the energy involved in this experiment (64 meV), a small fraction (10^{-4}–10^{-5}) of metastable atoms can survive the quenching process and be reflected by the repulsive part of the atom surface potential. It is

worth noticing that the quenching probability increases rapidly when the component of the atom velocity along the normal to the surface increases. In other words, the highest atom reflectivity is obtained when the angle between the He* beam and the grating is as small as possible and that is one of the reasons why the experiment is performed at grazing incidence. Of course, long counting times are also needed to get a good signal-to-noise ratio.

The second important point is the angular definition of the experiment. When considering an initial wave packet hitting the reflection grating (period Λ) at a given grazing incidence θ_i (see Fig. 1), the phase condition on the scattered wave packets imposes that the atomic signal is only expected at angles θ_N (with respect to the grating plane) fulfilling the condition

$$\cos\theta_N = \cos\theta_i - N\frac{\lambda_\parallel}{\Lambda} \tag{1}$$

where $\lambda_\parallel$ is the longitudinal de Broglie wavelength and N is the diffraction order. For the small incident angles considered here, equation (1) becomes

$$\theta_N^2 \approx \theta_i^2 + 2N\frac{\lambda_\parallel}{\Lambda}. \tag{2}$$

Typical experimental parameters are $\theta_i \approx 7$ mrad, $\Lambda = 2$ μm and, for He* atoms, $\lambda_\parallel = 0.057$ nm. Under these conditions, θ_N ranges from 7 to 14.8 mrad for $N = 0$ to 3. In order to resolve such close diffraction peaks, the overall resolution has to be better than 2 mrad. This condition is a priori fulfilled since the incident supersonic beam angular divergence is $\delta\theta \approx 0.35$ mrad, and the resolution of the position-sensitive detector is about 0.01 mrad. It will be still fulfilled after the treatment of the data which enlarges the angular spread up to $\Delta\theta = 1$ mrad FWHM.

It appears very important to know the θ_i value with accuracy in order to derive θ_N angles. At least for He* atoms, diffraction peaks only exist for $N \geqslant 0$ (otherwise Eq. (2) would give $\theta^2 < 0$). The first observable diffraction peak is then the $N = 0$ order (specular reflection). Notice that $\theta_{N=0}$ diffraction angle is the only one which does not depend on the incoming atom wavelength. This has been indeed observed by comparing He*, Ne* and Ar* diffraction patterns. From these experiments, we get $\theta_i = 7 \pm 0.3$ mrad.

Another important condition to observe diffraction effects is that the transverse coherence length of the wave packets covers several periods of the grating. As we are at grazing incidence, the effective transverse period of the grating, $\Lambda\theta_i$, is much smaller than Λ e.g. 14 nm instead of 2000 nm, for $\theta_i \sim 7$ mrad. The transverse coherence radius of our He* beam can be evaluated according to the van Cittert–Zernike theorem to be $R_c = 1660$ nm [8]. This means that, in the transverse plane, more than 100 slits can be covered by an incoming atomic wave packet.

Diffraction peaks are related to in-phase diffraction amplitudes. The last condition to observe them is that the outgoing wave packets scattered by consecutive grating periods do overlap each other. Actually wave packets spread when propagating, as $L_c[1 + (2z/k_\parallel L_c^2)^2]$, where z is the propagation distance, $k_\parallel$ the longitudinal wave number and L_c the longitudinal coherence length as defined before ($L_c = \lambda_\parallel v/\delta v$). Consequently the packets contain an increasing number of wavelengths. Nevertheless their overlap does not depend on the distance along which they propagate. Then the condition of overlapping can be simply written as $-L_c < \Delta < L_c$ where $\Delta = N\lambda_\parallel$ is the path difference between two in-phase outgoing wave packets, N being an integer. Here we can observe an in-phase scattered signal only for $N < 50$–100. Such maximum diffraction orders are far above the experimental range. One can notice that the observable diffraction orders depend on the quality of the velocity distribution ($\delta v/v$) since the overlapping condition can also be written $N < v/\delta v$. This means that, as expected, the more monokinetic the beam is, the more orders of diffraction are seen.

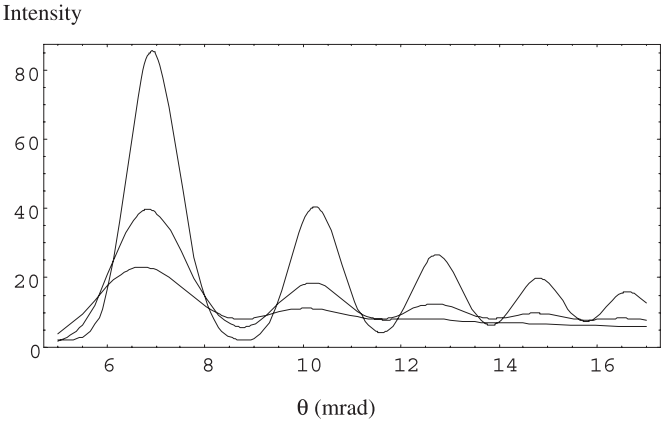

Fig. 2. Simulation of the effects of different random roughness (rms value $\sigma = 2$, 3 and 5 nm (see text)) on the diffraction pattern of He* on a reflection-grating of $\Lambda = 2$ μm. The most contrasted pattern is obtained for $\sigma = 2$ nm, the less contrasted one for $\sigma = 5$ nm. However, for $\sigma \leqslant 3$ nm, one can clearly see diffraction peaks up to order 3. For the gratings used in these experiments, the manufacturer gives $\sigma \leqslant 2$ nm.

Finally, we have to consider the problem of the grating surface roughness. A simulation of the roughness effect can be carried out considering a random height ξ of the reflecting surface above an ideal plane, the distribution of which is Gaussian, with a standard deviation σ. This roughness generates a random phase $\eta = \delta k\, \xi$, where $\delta k \approx k\theta$ is the momentum change along the normal to the surface, θ being the scattering angle. The η-standard deviation is then $k\theta\sigma$. As a function of the total phase shift $\Phi + \eta$, where $\Phi \approx \frac{1}{2}\Lambda k(\theta^2 - \theta_i^2)$ refers to an ideal grating of period Λ, the intensity becomes a random signal $I(\Phi + \eta)$. The statistical average of this signal is $\bar{I}(\Phi) = \int_{-\infty}^{+\infty} I(\Phi + u)g(u)du$, where $g(u)$ is the Gaussian probability density of η. Here $I(\Phi)$ represents the diffraction pattern of the ideal grating, which is actually an *interference* pattern produced by p active mirrors ($p \gg 1$). The contrast of the fringes, equal to the degree of coherence, is 1 in this ideal case. However, the diffraction pattern is damaged by roughness: the contrast (or visibility) is reduced. Figure 2 shows resulting diffraction patterns for He* atoms ($k = 5.83$ a.u.), with

$\sigma = 2$ nm, 3 nm and 5 nm. It is seen that for $\sigma \leqslant 3$ nm (the manufacturer gives $\sigma = 1$–2 nm), diffraction peaks remain visible up to order 3.

2.3 Experimental device

The experimental set up is the following: the metastable atom supersonic beam is twice collimated as mentioned before. The grating is set at 597 mm from the nozzle (the point-like atomic source of the experiment) on a rotating holder which allows us to tune the incidence angle (θ_i) of the beam on the grating from 0 to 10 mrad. We detect the signal on a position-sensitive detector which is set at 1396 mm from the nozzle. This detector consists of a multichannel electron multiplier followed by a phosphor screen and a CCD camera. The estimated overall spatial resolution is 7 μm which corresponds to an angular resolution of 0.01 mrad.

The home-made reflection gratings used here present several advantages: (i) they are inexpensive, (ii) the size of reflecting structures is relatively large (typically hundreds of nm), (iii) a wide variety of shapes and sizes are available (this type of fabrication has already been used by Shimizu et al. [1] in atom holography experiments), (iv) deposited structures are controlled using an atomic-force microscope, (v) the technique is usable with various non-magnetic and magnetic materials. The non-magnetic reflection grating used here (called in the following G1) consists of thin bars of aluminium deposited on a silicon substrate through a resist mask realized by electron beam lithography in a scanning electron microscope (lift-off technique [15]). The width of the bars is 500 nm, their thickness is 30 nm and the separation between two consecutive bars is 1500 nm (period $\Lambda = 2$ μm). The bars are set perpendicular to the atomic beam axis so that atoms are expected to diffract in the vertical direction (Fig. 1). The "magnetic" grating consists of thin stripes of Permalloy (thickness $e = 30$ nm, width $w = 1500$ nm, period $\Lambda = 1800$ nm) deposited on a silicon substrate. The technique of deposition combines electron-beam lithography and ion-beam etching [16]. The Permalloy material is known to have a high relative magnetic permeability ($\mu > 8000$) and a small residual magnetisation. This latter property is important since it will allow to use this grating as a non-magnetic structure (called G2) when no external magnetic field is applied, or as a magnetised one (G2m) as soon as a magnetic field is applied. One can see a Scanning Electron Micrograph (SEM) of grating G2 in Figure 3.

Fig. 3. Scanning Electron Micrograph of the magnetic grating G2 (see text) of period $\Lambda = 1.8$ μm and width $w = 1.5$ μm.

3 Results and discussion

3.1 Non-magnetic gratings

An angular diffraction pattern is obtained for He* atoms, at $\theta_i \approx 7$ mrad, with grating G1. It consists of 500 accumulated images. A vertical cut of the pattern is taken (see Fig. 4a). A background signal due to the CCD device (about 10 counts/image) is subtracted. A smoothing averaging method is used to better extract diffraction peaks from the residual background signal. Indeed it reduces the statistical noise by a factor 3.9. Its counterpart is to add 0.7 mrad to the angular width (originally of about 0.4 mrad) of the diffraction peaks. Only positive angles are shown as atoms can only diffract in the ascendant direction. Indeed, the grating acts as a mask for atoms diffracting downwards. Angles smaller than 5 mrad have been ignored because of the very high magnitude of the central peak (a few thousands times the diffraction peak magnitudes) and possible diffraction effects due to the edge of the grating holder. One can clearly see diffraction peaks in Figure 4a (vertical arrows). The same experiment has been carried out with Ne* and Ar* beams (see Figs. 4b and 4c).

According to formula (2), one can then plot the location θ_N^2 of diffraction peaks as a function of the diffraction order N. These locations should then lie on a straight line passing through the point $\theta_0^2 = \theta_i^2$, the slope of which is $2\ \lambda_\parallel/\Lambda$. In Figure 5 the results are shown for He* (full triangles), Ne* (full squares) and Ar* (open circles), together with predicted straight lines. The agreement can be considered as rather good, the remaining discrepancy being probably due to errors in the largest scattering angle determination (θ_N angles are measured at ± 0.5 mrad, which leads to an uncertainty of ± 17.3 mrad^2 on θ_N^2 at $\theta_N^2 = 300$ mrad^2). Similar results are obtained with the demagnetised magnetic grating (G2). They will be discussed further in view of a comparison with those given by the magnetised version of the same grating (G2m).

As in the case of transmission gratings, the diffraction amplitude is the product of a universal grating amplitude, $\sin[(p+1)\varphi/2]/\sin[\varphi/2]$, where p is the number of active slits and φ the phase-shift between 2 consecutive slits, by the diffraction amplitude of a single slit, or a single stripe in our case. Only this latter amplitude involves the atom-solid interaction. It appears in the diffraction pattern as an envelope of the grating diffraction peaks. For non-magnetic gratings, the atom-metal interaction at mean distance (0.5–100 nm) is of the van der Waals type. In the case of metastable helium atoms (He* 2 ^{3,1}S$_{1,0}$)

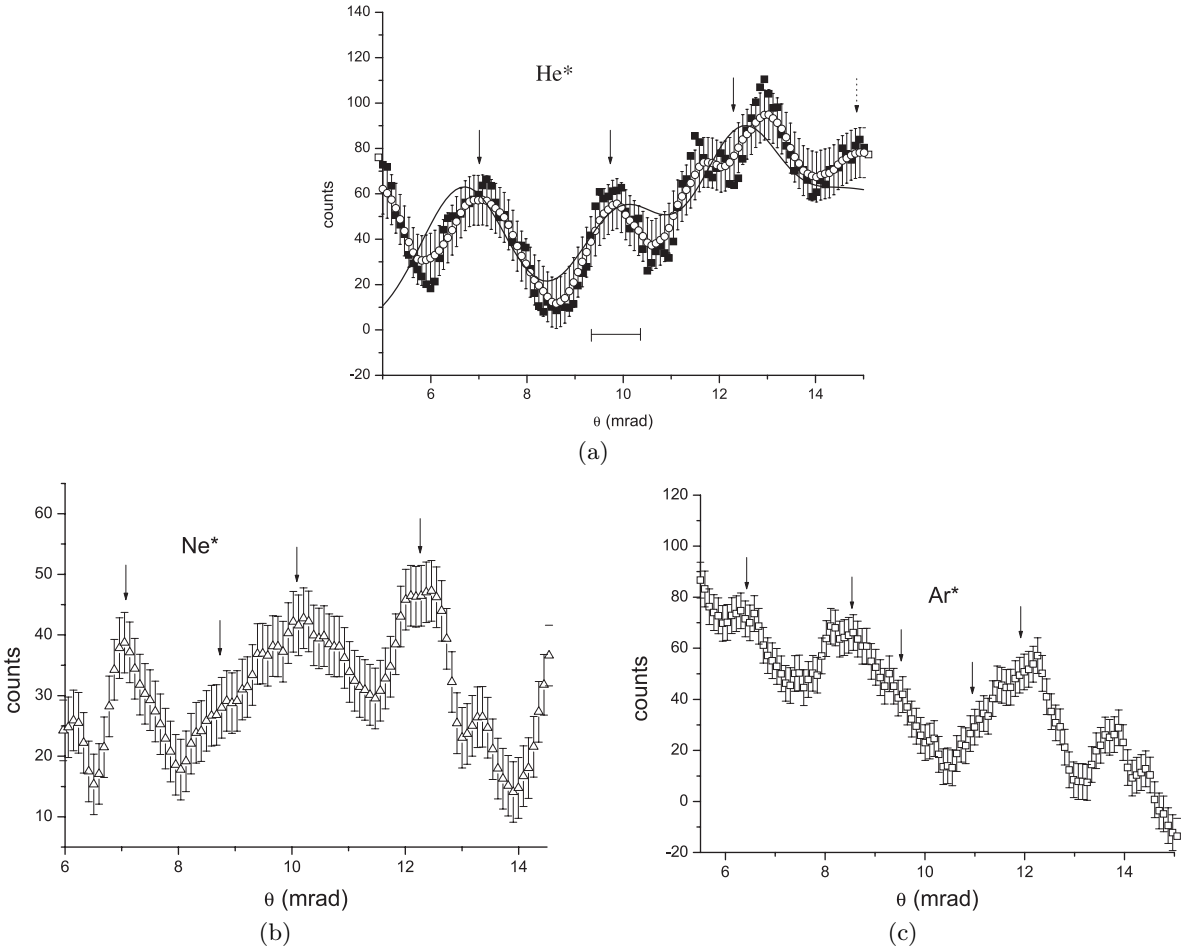

Fig. 4. (a) Spectrum of the vertical angular distribution of a 1750 ms^{-1}-He^* beam, diffracted by a non magnetic reflection grating (G1, period $\Lambda = 2$ μm). Only positive angles, larger than 5 mrad, are shown (see text). Diffraction peaks are indicated by vertical arrows. The peak at zero angle (not shown) corresponds to atoms passing above the grating; its intensity is about 1000 times larger than diffraction peaks. Two steps of averaging are shown (open circles data are issued from an adjacent averaging 1.6 times stronger than the weak averaging used to obtain the full squares data). The uniform vertical error bar ($\pm$11 counts) represents the spreading of data points before final averaging. The horizontal bar represents the convolution window due essentially to the averaging process ($\Delta\theta = 1$ mrad). Full line: calculated diffraction pattern including the vdW potential effect and the averaging process. (b) Spectrum of the vertical angular distribution of a 780 ms^{-1}-Ne^* beam, diffracted by grating G1 (period $\Lambda = 2$ μm). (c) Spectrum of the vertical angular distribution of a 560 ms^{-1}-Ar^* beam, diffracted by grating G1 (period $\Lambda = 2$ μm).

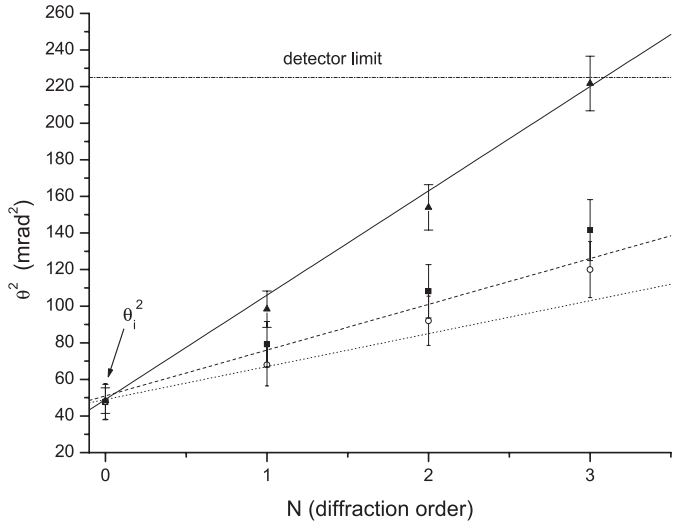

Fig. 5. Location of diffraction peaks produced by grating G1 (see text), in a diagram (θ^2, N) where N is the diffraction order. He^* (full triangles: data; full line: theoretical prediction). Ne^* (full squares: data; dashed line: theoretical prediction). Ar^* (open circles: data; dotted line: theoretical prediction). The value $\theta^2(N = 0) = \theta_i^2 = 49$ mrad^2 is independent of the atomic wavelength and then identical for the 3 atoms. Error bar at a given angle θ is $2\theta\Delta\theta$. The spatial detector limit is $\theta_{lim} = 15$ mrad, i.e. $\theta_{lim}^2 = 225$ mrad^2.

this attractive interaction is essentially scalar, decreasing as x^{-3}, where x is the atom-surface distance (see Fig. 1). At short distance, because of the overlap of the atomic external orbital with metal-electron orbitals, the interaction becomes a repulsive one (in x^{-9} in average). It should be noticed that this potential, responsible for the reflection, has the same distance range as the coupling responsible for the quenching of the metastable atoms. The total He* atom-metal interaction $V(x)$ has been calculated using the van der Waals constant $C_3 = 1.31$ a.u. (i.e. 1.27 kHz μm^3) derived from diffraction data [8,9] and, for the repulsive contribution, a transposition of the Zaremba and Kohn method [17] to the case of He* [10]. The quantity $U(x) = 2mV(x)$, where m is the atomic mass, is given (in atomic units) by:

$$U(x) = -1.9225 \times 10^4 x^{-3} + 2.46702 \times 10^9 x^{-9} \qquad (3)$$

(see Fig. 6a). In a transmission configuration, the semi-classical phase-shift related to a given trajectory is rather easy to evaluate because a rectilinear unperturbed trajectory can be considered as a zero-order approximation. Such a reference is no longer available in the reflection mode where the distance of closest approach depends on the angles (θ, θ_i) under consideration. The problem is greatly simplified when the repulsive part of the interaction is assimilated to an infinite wall located at a finite distance x_0 (here $x_0 \approx 7.1$ a.u.). Indeed in such a case the distance of closest approach is identical to x_0 and an attractive potential $W(\xi)$, symmetric in $\xi = x - x_0$, can be used to evaluate the phase-shift. This phase-shift, $\phi(X, Z)$, is between a trajectory (2 branches asymptotically inclined by θ and θ_i) passing by a point of co-ordinates X (normal to the surface) and Z (parallel to the surface), and a similar trajectory passing by point (0, 0). It can be written as:

$$\phi(X, Z) \approx k_\parallel(\cos\theta - \cos\theta_i)Z + [\mathrm{K}(\xi) - k_\parallel]\xi(\sin\theta + \sin\theta_i) \qquad (4)$$

where $K(\xi) = \nu(\xi)k_\parallel$, ν being the semi-classical index: $\nu(\xi) \approx [1 + W(\xi)/k_\parallel^2]^{1/2}$. For He* atoms, $k_\parallel = 5.83$ a.u. The amplitude diffracted by one stripe is then:

$$f(\theta) \propto \int_{-\infty}^{+\infty} dX \int_{-w/2}^{+w/2} dY \exp[i\phi(X, Y)] = w\frac{\sin[(\cos\theta - \cos\theta_i)k_\parallel w/2]}{(\cos\theta - \cos\theta_i)k_\parallel w/2} \times \int_{-\infty}^{-\infty} d\xi \exp[ik_\parallel(\sin\theta + \sin\theta_i)(\nu(\xi) - 1)\xi] \qquad (5)$$

where w (500 nm for G1, 1500 nm for G2) is the width of the stripe. The calculated diffraction pattern of He* atoms for grating G1 at an incidence $\theta_i = 7$ mrad is shown in Figure 4 together with experimental data. This calculation takes in account the finite angular spread, using a convolution by a Gaussian profile. The agreement can be considered as rather satisfactory owing to the huge simplifications introduced in the calculation (infinite abrupt wall, zero interaction outside the stripe) and to the experimental uncertainties.

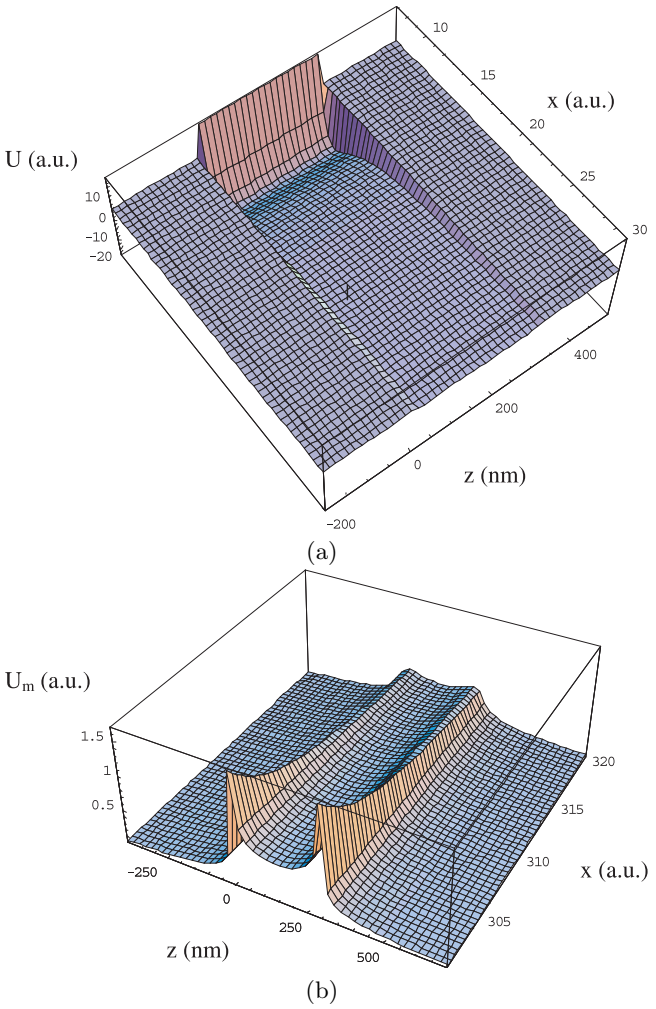

Fig. 6. (a) Reduced atom-surface potential U (see text) across a bar (z-coordinate) of non-magnetic grating (G1), as a function of the distance x to the surface. (b) Reduced magnetic potential U_m (see text) across the gap between two consecutive magnetic bars (z-coordinate) (grating G2m), as a function of the distance x to the surface.

3.2 Magnetic grating

The grating, the plane (y, z) of which is almost horizontal, is placed within a vertical homogeneous static magnetic field $\mathbf{B}_0$ (250 G in magnitude), parallel to x-axis. Assuming a linear response, the magnetisation $\mathbf{M}$ is collinear to $\mathbf{B}_0$ and it is given by: $\mu_0\mathbf{M} \approx (1 - \mu_0/\mu)\mathbf{B} \approx \mathbf{B}$ where $\mathbf{B}$ is the total magnetic field. The field $\mathbf{B}'$ generated by a stripe can be obtained from the surface-current density $\mathbf{J} = \mathbf{M} \times \mathbf{n}$ where $\mathbf{n}$ is the outer normal to the solid. $\mathbf{J}$ is anti-parallel to y-axis on the gap border $z = 0$ and parallel

to it on the border $z = w$. The components of $\mathbf{B}'$ are easily derived in the form: $B'_x = BF(x,z)$; $B'_z = BG(x,z)$, where F and G are well defined analytic functions:

$$F = (2\pi)^{-1}[\mathrm{Arctg}[x/z] + \mathrm{Arctg}[(e-x)/z] - \mathrm{Arctg}[x/(z-w)] - \mathrm{Arctg}[(e-x)/(z-w)]]$$

$$G = (4\pi)^{-1}\mathrm{Log}\left[\frac{x^2+z^2}{e^2+z^2-2ex+x^2} \times \frac{e^2+(z-w)^2-2ex+x^2}{x^2+(z-w)^2}\right]. \quad (6)$$

The unknown value of B appears as the positive root of the equation: $B^2 = B^2G^2 + (B_0 + BF)^2$, namely $B = B_0[(1-G^2)^{1/2} + F]/(1-F^2-G^2)$. This readily gives $B' = B(F^2+G^2)^{1/2}$. Once the $He^*(2\ ^3S_1)$ atom, in its magnetic sub-level $M = -1$, is entered into the homogeneous field B_0 (with a negligible loss of kinetic energy), it experiences a repulsive magnetic potential $V_m = +|g|\mu_B B'$, where $g = -2$ is the Landé factor and μ_B the Bohr magneton. The magnitude of B' is everywhere large enough to ensure an adiabatic evolution of the atomic spin. The shape of the product $U_m = 2mV_m$, where m is the atom mass, is shown in Figure 6b. It is seen that the potential is sharply peaked along both edges of the 300 nm gap between two magnetised stripes, with a magnitude higher than the normal kinetic energy. This can be viewed, in a very simplified approach, as making atoms rebound on 2 narrow mirrors (the width of which is a few 10 nm) placed along both edges of a gap. Under such condition, the single-structure diffraction pattern is the counterpart, in the reflection mode, of the 2 Young's slit interference pattern. It yields the envelop of the complete grating diffraction pattern. In Figure 7, experimental and calculated diffraction patterns produced by non-magnetised (G2) and magnetised (G2m) versions of the same grating, are compared. The calculation for G2 is the same as that already given for G1, whereas the calculation for G2m uses the simple previous model. The most striking feature is the observed strong reduction of the order 2 induced by the magnetic potential, as predicted by the theoretical calculation.

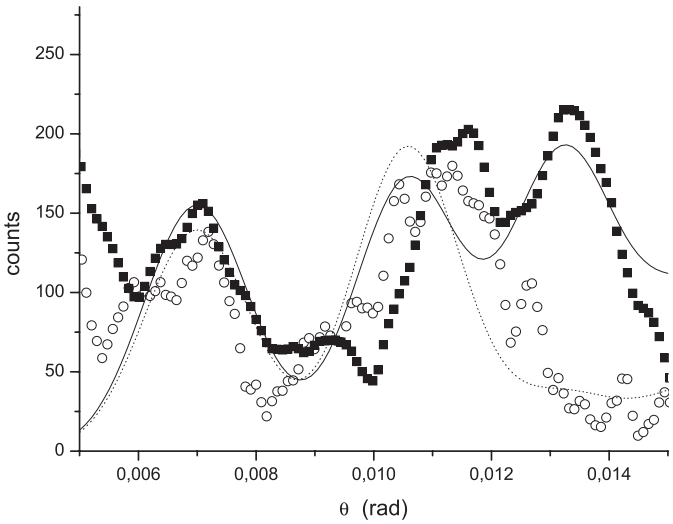

Fig. 7. Spectra of the vertical angular distribution of a 1750 ms^{-1}-He^* beam diffracted by a magnetic reflection grating (period $\Lambda = 1.8$ μm). The grating (G2m) is magnetized by a uniform field of 250 G (open circles: experimental data; dotted line: calculated diffraction pattern) or not magnetized (G2) (full squares: data; full line: calculated diffraction pattern). One may notice that when the magnetic field is applied, the second diffraction order is strongly reduced (see text).

4 Conclusion and perspectives

We have demonstrated, for the first time to our knowledge, the 1D-diffraction of thermal velocity metastable rare gas atoms by non-magnetic and magnetic micro-metric reflection gratings. In spite of fundamental difficulties (high quenching factor of metastable atoms hitting the grating, smallness of the de Broglie wavelength of fast atoms), the occurrence of the phenomenon is experimentally clear. Although the phenomenon was theoretically predictable, it was important to show experimentally that diffraction of fast atoms by micro-metric reflection gratings, and not only that of cold atoms, is indeed observable. Experiments using 2D-gratings, which produce 2D-diffraction patterns observable on a position-sensitive detector, are in progress. They are expected to be a preliminary step towards fast atom holography in the reflection mode.

At a more practical level, this demonstration is useful because reflection gratings do not need to be structured at a nano-metric scale, and they are far easier to produce (and buy) than nano-transmission gratings. Experimentalists thinking of coherent splitting of a fast atom beam using elastic diffraction can now consider using fabricated reflection gratings. It is worth noticing that "fast" atoms (i.e. atoms at thermal velocity) are not necessarily the best candidates. Slower atoms present some advantages, but the point here is that moderate velocities (a few tens of m/s), not very small ones, would be quite convenient for this type of experiments.

The same kind of technique can be used as a probe of the grating surface. Indeed, as the diffraction pattern depends on the surface potential, one can obtain information about various atom-surface interactions (van der Waals and Casimir Polder interactions, magnetic interaction, etc.). This information is contained in the envelope of the diffracted peaks, which remains so far difficult to estimate because of the low signal due to the quenching factor, at least in the case of non-magnetic surfaces. In spite of that, we have shown here the feasibility of such a treatment. Overcoming this difficulty, for instance by slowing the atoms down to a moderate velocity, 1D and 2D diffractions of atoms by micro-metric reflection gratings appear to be a very interesting tool for atom-surface interaction spectroscopy. Another way to eliminate the quenching effect would be to operate with a beam of ground state atoms, and then use the metastability exchange process

to reveal and detect image diffraction or interference patterns. This technique is expected to be feasible owing to the efficiency of the metastability exchange in producing the present incident beam.

References

1. F. Shimizu, J. Fujita, Phys. Rev. Lett. **88**, 123201 (2002)
2. O. Stern, Naturwiss. **17**, 391 (1929); I. Estermann, O. Stern, Z. Phys. **61**, 95 (1930)
3. P. Cantini et al., Phys. Rev. B **19**, 1161 (1979)
4. M. DeKieviet et al., Surf. Sci. **365**, 789 (1996)
5. G. Brusdeyling et al., Phys. Rev. Lett. **44**, 1417 (1980)
6. D.W. Keith et al., Phys. Rev. Lett. **66**, 2693 (1991)
7. R.E. Grisenti et al., Phys. Rev. Lett. **83**, 1755 (1999)
8. J.-C. Karam et al., J. Phys. B: At. Mol. Opt. Phys. **38**, 2691 (2005)
9. R.Brühl et al., Europhys. Lett. **59**, 357 (2002)
10. J.-C. Karam et al., Europhys. Lett. **74**, 36 (2006)
11. J.F. Clauser, Physica B **151**, 262 (1988)
12. R. Deutschmann et al., Phys. Rev. A **47**, 2169 (1993)
13. R. Campargue, J. Phys. Chem. **88**, 4466 (1984)
14. W. Sesselmann et al., Phys. Rev. B **35**, 1547 (1987)
15. Y. Oshiai, M. Baba, H. Watanabe, S. Matsui, Jap. J. Appl. Phys. **30**, 3266 (1991), and references therein
16. S.M. Chérif, J.F. Hennequin, J. Magn. Magn. Mat. **165**, 504 (1997)
17. E. Zaremba, W. Kohn, Phys. Rev. B **15**, 1769 (1977)